



## Durable and highly-efficient anion exchange membrane water electrolysis <sup>1</sup> using poly(biphenyl alkylene) membrane



Zhangtang Jiang <sup>a,b</sup>, Guiqin Yi <sup>a</sup>, Xin Yao <sup>a</sup>, Yichang Ma <sup>a,b</sup>, Xiangyu Su <sup>a,b,\*</sup>, Qinglin Liu <sup>a,2</sup>, Qiugen Zhang <sup>a,b,\*</sup>

<sup>a</sup> State Key Laboratory for Physical Chemistry of Solid Surfaces, College of Chemistry & Chemical Engineering, Xiamen University, Xiamen 361005, China <sup>3</sup>

<sup>b</sup> Fujian Science & Technology Innovation Laboratory for Energy Materials of China (IKKEM), Xiamen 361102, China

### ARTICLE INFO <sup>4</sup>

**Keywords:**  
Anion exchange membrane <sup>6</sup>  
Water electrolysis  
Hydrogen production  
Poly(biphenyl alkylene)  
Poly(arylene) membrane

### ABSTRACT <sup>5</sup>

Anion exchange membrane water electrolysis (AEMWE) is a promising technology for large-scale green-hydrogen production, owing to high current density, low gas permeability and low capital cost. High-performance and durable anion exchange membrane (AEM) is the key to bringing it into practical utilization. In this study, poly(biphenyl alkylene) (PBPA) AEM is synthesized and used for the highly-efficient and durable AEMWE. The fabrication conditions of membrane electrode assembly (MEA) and working condition of water electrolysis are investigated in detail. The ionomer contents and electrolyte type significantly affect the performance and durability of the PBPA-based AEMWE cell. The as-fabricated AEMWE cell with the PBPA membrane achieves a current density as high as  $4.0 \text{ A cm}^{-2}$  @ 2.0 V in 1 M KOH at 80 °C and a continuous water electrolysis of over 3,500 h at  $1.0 \text{ A cm}^{-2}$  with a slow voltage rising rate of  $6.5 \mu\text{V h}^{-1}$ . The high performance and long durability exhibit that the PBPA-based AEM is promising towards the industrial hydrogen production. <sup>7</sup>

### 1. Introduction <sup>8</sup>

Developing and utilizing renewable energy technologies (e.g., solar <sup>9</sup> cells, wind power and fuel cells) are recognized as the most feasible route to address the energy and environmental problems [1,2]. Water electrolysis, which utilizes renewable electricity to produce hydrogen as fuel or chemical raw material, will be an indispensable part of the upcoming renewable energy system [3,4]. Although traditional water electrolysis has been commercialized for more than 100 years, its further application is limited by the low energy efficiency and high explosion risk [5]. To meet the next-generation requirements of hydrogen production, advanced water electrolysis technologies that exhibit high energy efficiency, compact structure and much better gas separation have been extensively developed [6–8]. Among them, AEMWE not only possesses high performance and safety, but also inherits low precious metal use and high contamination tolerance from traditional alkaline water electrolysis [9,10]. Therefore, the powerful and cost-effective AEMWE will be highly competitive in the future large-scale hydrogen production of water electrolysis [11,12].

In the development of AEMWE, considerable progress has been made <sup>10</sup>

based on the advanced AEMs. For instance, Cha *et al.* reported a series of poly(carbazole) AEMs for the AEMWE, which achieves a current density of  $3.5 \text{ A cm}^{-2}$  @ 1.9 V (1.0 M KOH, 70 °C) [13]. Holdcroft *et al.* reported the AEMWE cell with a methylated polybenzimidazole AEM that has a current density of  $2.0 \text{ A cm}^{-2}$  @ 1.82 V (1.0 M KOH, 60 °C) [14,15]. Kim *et al.* reported an AEMWE cell based on alkylammonium polyphenylene AEM, which has current densities of  $2.7 \text{ A cm}^{-2}$  and  $5.5 \text{ A cm}^{-2}$  at 1.8 V and 85 °C with pure water and 1.0 M KOH solution, respectively [16]. Although many AEMWE cells show high current density, it is still a challenge to meet the requirement of industrial hydrogen production due to their limited durability. The durability of AEMWE mainly depends on the chemical stability of the AEMs in alkaline working condition. Although many efforts were devoted to the development of alkali-resistant AEMs in the past decade, few AEMWE cells equipped with the high-performance AEM achieved durable hydrogen production for more than 1000 h [4,9,17,18]. Therefore, high-performance and durable AEMs are urgently needed for industrial AEMWE development. <sup>11</sup>

Linear aromatic polymers, synthesized by super electrophilic acid-catalyzed Friedel-Crafts polycondensation, have attracted a lot of attention in the development of durable AEMs, owing to the resulting <sup>12</sup>

\* Corresponding authors at: State Key Laboratory for Physical Chemistry of Solid Surfaces, College of Chemistry & Chemical Engineering, Xiamen University, Xiamen 361005, China.

E-mail addresses: [Xysu@xmu.edu.cn](mailto:Xysu@xmu.edu.cn) (X. Su), [qgzhang@xmu.edu.cn](mailto:qgzhang@xmu.edu.cn) (Q. Zhang).

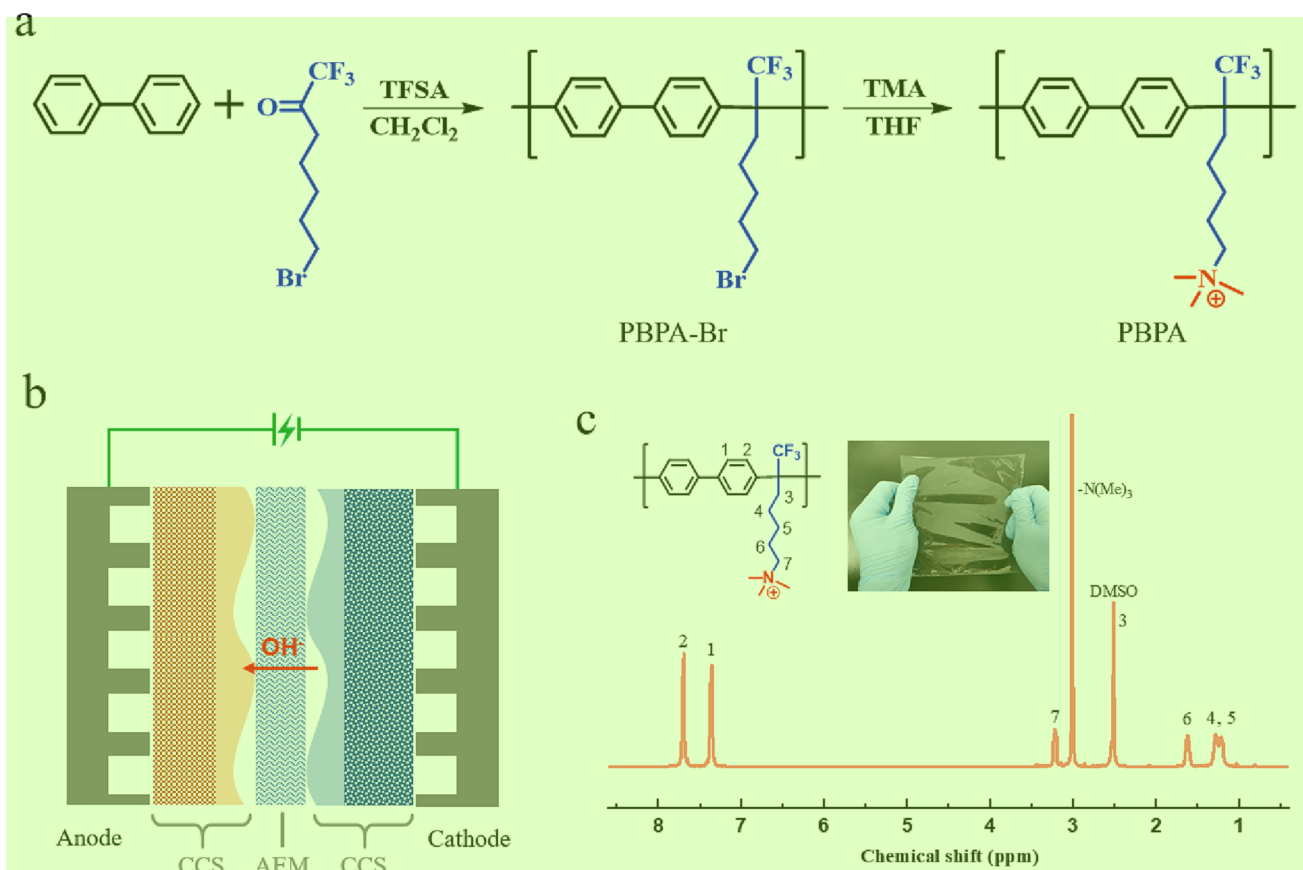


**Fig. 1.** Synthesis of PBPA AEM for the AEMWE. a) Synthesis route of the PBPA. b) Illustration of assembled AEMWE cell. c)  $^1\text{H}$  NMR spectrum of as-synthesized 2 PBPA, with the inset of a photo of PBPA AEM. 3

all-carbon backbone, flexible side chains terminated by cation head groups, narrow polydispersity and ultrahigh molecular weight [11,19–24]. As a representative, poly(biphenyl alkylene) (PBPA) AEM has a high hydroxide ion conductivity of  $122 \text{ mS cm}^{-1}$  at  $80^\circ\text{C}$ . After immersing in  $1.0 \text{ M NaOH}$  solution at  $95^\circ\text{C}$  for 60 days, only 8.0% of ion exchange capacity (IEC) dropped, exhibiting remarkable chemical stability [20,23]. Unlike many polymers with electron-withdrawing groups (such as aryl ether bond, carbonyl group, sulfonyl group, etc.), the repeating unit of the PBPA backbone is a rigid biphenyl and a methine, which can effectively prevent the attack of hydroxide. Meanwhile, attaching trimethylamine cationic groups to the polymer backbone with a long alkyl side chain, the prepared polyelectrolyte can obtain good alkali stability [25–28]. It should be a good candidate for the highly-efficient and durable AEMWE. Moreover, the synthesis is facile and cost-effective.

In this study, the PBPA AEM was synthesized (Fig. 1a) and fully characterized for the AEMWE. The effects of several key factors on the water electrolysis performance were investigated in detail, including ionomer contents, type and concentration of electrolyte solution, and operating temperature. Finally, long-term constant current electrolysis (CCE) test of 3,500 h was performed in  $1.0 \text{ M KOH}$  at  $1.0 \text{ A cm}^{-2}$  and  $60^\circ\text{C}$ , and the average increase of the cell voltage was only  $6.5 \mu\text{V h}^{-1}$ . The PBPA-based cell using the nonprecious  $\text{NiFe}_2\text{O}_4$  anode catalyst was also investigated and presented.

## 2. Experimental section 5

### 2.1. Synthesis of PBPA AEM 6

The PBPA with quaternary ammonium groups was synthesized according to the literature [20]. As shown in Fig. 1a, the PBPA with

3 bromine groups (PBPA-Br) was synthesized by superacid catalyzed 8 Friedel-Crafts polycondensation from biphenyl and 7-bromo-1,1,1-trifluoroheptan-2-one (99 wt%, Xiamen Kah Membrane Technology Ltd.) in the presence of trifluoromethanesulfonic acid (TFSA) (J&K Scientific), and then was functionalized by trimethylamine in tetrahydrofuran at room temperature.

The PBPA AEM was prepared by traditional solution-casting method 9 [22]. The obtained PBPA was dissolved in dimethylsulfoxide and then filtered by polytetrafluoroethylene filters with a cut-off of  $0.45 \mu\text{m}$  (Sinopharm Chemical Reagent Co., Ltd.). The resulting 5 wt% PBPA solution was uniformly cast on clean glassy mold plates, and then heated for 12 h at  $60^\circ\text{C}$  and another 8 h at  $120^\circ\text{C}$  in a vacuum oven. Finally, the PBPA AEMs with a thickness of  $50 \mu\text{m}$  were obtained.

### 2.2. Preparation of MEA 10

The MEA was assembled by sandwiching a PBPA AEM with an anode and a cathode, as shown in Fig. 1b. The catalyst-coated-substrate (CCS) electrodes were prepared by air-spraying method. The  $0.2 \text{ mm}$ -thick nickel foam (Xiamen Kah Membrane Technology Ltd.) and hydrophilic carbon paper (TGP-H-060, Toray Industries, Inc.) were used as the anode and cathode substrates, respectively. Commercial  $\text{IrO}_2$  (99.8 wt%, Suzhou Sinero Technology Co., Ltd.) and  $\text{Pt/C}$  (60 wt%, Johnson Matthey Co., Ltd.) nanoparticles were employed as the anode and cathode catalysts, respectively. In each catalyst ink preparation, appropriate amount of AEI was ultrasonically mixed with appropriate amounts of catalyst and water/isopropanol (1:1) solution. A catalyst loading of  $1.0 \text{ mg cm}^{-2}$  was employed for both the anode and cathode. Anodes with AEI contents of 2.5, 5.0, 7.5, 10.0, 12.5 and 15.0%, respectively, were fabricated. Cathodes with AEI contents of 15, 20, 25, 30 and 35%, were also prepared respectively. Another nonprecious anode was also fabricated

**Table 1**  
Properties of 50  $\mu\text{m}$ -thick PBPA AEM.

Property	Condition	Value
IEC ( $\text{mmol g}^{-1}$ )	—	2.60
Tensile strength (MPa)	dry	35
	wet	15
Elongation at break (%)	dry	55
	wet	95
Water uptake (%)	30 °C	121
	60 °C	132
	80 °C	140
Swelling ratio (%)	30 °C	39
	60 °C	42
	80 °C	44
$\text{OH}^-$ conductivity ( $\text{mS cm}^{-1}$ )	30 °C	60
	60 °C	84
	80 °C	123

using the same method, with 1.5  $\text{mg cm}^{-2}$  nonprecious catalyst (Kmem® AC01, Xiamen Kah Membrane Technology Ltd.).

### 2.3. Characterizations

The synthesized PBPA was characterized via nuclear magnetic resonance (NMR) spectroscopy (AVANCE NEO 500, Bruker). The molecular weight and its distribution were measured by gel permeation chromatography (GPC) (Waters 1515, Waters). Properties of PBPA AEM, including IEC, water uptake, swelling ratio, ion conductivity, mechanical strength, elongation, and thermal stability were characterized according to our previous study [22]. The hydrogen permeability of PBPA AEM was measured using a MEA cell [29]. As a comparison, the commercial Sustainion X37-50 membrane (Dioxide Materials) was tested as well. Micromorphology images of two typical as-prepared CCS electrodes were captured via scanning electron microscope (SEM) (GeminiSEM 500, Zeiss). The electrochemical surface area (ECSA) of typical anode and cathode was determined using a double layer capacitance method [30–32]. More details of these characterization methods are provided in the Supporting Information.

### 2.4. Water electrolysis experiments

The water electrolysis experiments of PBPA AEM were performed on a single-cell AEMWE instrument (Kmem® AE01, Xiamen Kah Membrane Technology Ltd.) (Fig. S1). The instrument integrates a single-cell fixture, heaters and a dual-channel circulating pumps, allowing for accurate

controls on the temperature and flow rate. The AEMWE cell was assembled by sandwiching the prepared MEA between bipolar plates with appropriate fastening. Each polar plate possesses a single-channel serpentine flow field (Fig. S1) in a square area of  $2 \times 2 \text{ cm}^2$ . Before the test, pretreatment of the AEI and AEM was conducted by circulating 200 mL 1.0 M KOH solution through the cell for 4.0 h at 60 °C.

The polarization test and CCE test were conducted using a battery test station (CT5001A, Wuhan LAND Electronic Co., Ltd.). The electrochemical impedance spectroscopy (EIS) test was performed on an electrochemical station (VersaSTAT 3F, AMETEK). In general, the CCE test was performed for 12 h. The EIS test was performed at the current density of 1.0  $\text{A cm}^{-2}$ . Typically, the electrolyte solution was circulated through both anode and cathode at a flow rate of 3.0  $\text{mL min}^{-1}$  at 60 °C. The long-term CCE test was performed in 1.0 M KOH at 1.0  $\text{A cm}^{-2}$  and 60 °C for 3,500 h.

## 3. Results and discussion

### 3.1. Properties of AEM and MEA

Structure and purity of the PBPA was confirmed via  $^1\text{H}$  NMR spectrum (Fig. 1c). The molecular weight was measured by GPC, having weight average weight ( $M_w$ ), number average weight ( $M_n$ ), and polydispersity ( $M_w/M_n$ ) are 73.09, 46.01, and 1.59, respectively (Fig. S2). The obtained 50  $\mu\text{m}$ -thick PBPA AEM is transparent and flexible (the inset of Fig. 1c). Its key properties, i.e., IEC, water uptake, swelling ratio, and hydroxide ion conductivity at 30, 60 and 80 °C were listed in Table 1. At 80 °C, the PBPA AEM exhibits a high hydroxide conductivity of 123  $\text{mS cm}^{-1}$ , water uptake of 140% and swelling ratio of 44%, which agrees with previous studies [20]. The PBPA AEM exhibits decent tensile strength of 35 MPa and elongation at break of 55% in the dry state (Fig. 2a). In comparison, the elongation at break in the wet state increases to 95%. Although the tensile strength decreases distinctly, it is still greater than 15 MPa and thus can meet the requirements of AEMWE [17].

As presented in Fig. 2b, the  $\text{H}_2$  permeation current density of PBPA AEM is much lower than the commercial Sustainion X37-50 AEM. According to calculation, the  $\text{H}_2$  permeabilities of these two membranes are 50 and 230  $\text{pmol cm}^{-2} \text{s}^{-1}$ , respectively. The thermal behavior of PBPA AEM was evaluated by thermogravimetric analysis (TGA) and dynamic mechanical analysis (DMA), as shown in Fig. S3. It is found that the first decomposition temperature is around 250 °C due to the loss of quaternary ammonium groups, and further decomposition occur at 450

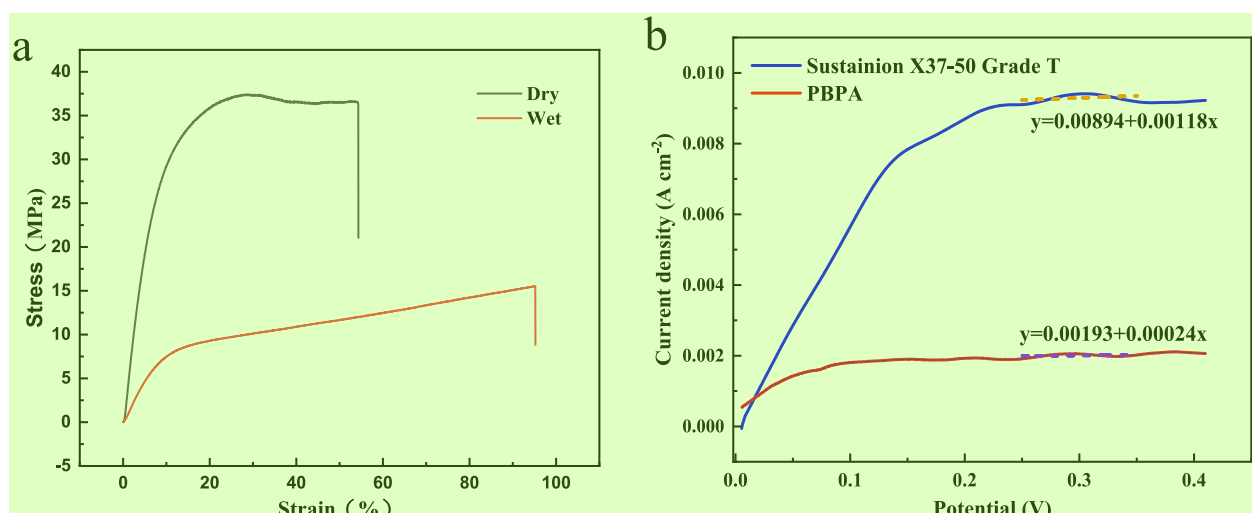


**Fig. 2.** Mechanical properties and hydrogen permeability of PBPA AEM. (a) Tensile curves of the PBPA AEM in dry and wet state. (b) Hydrogen permeation current densities of PBPA and Sustainion X37-50 AEMs.

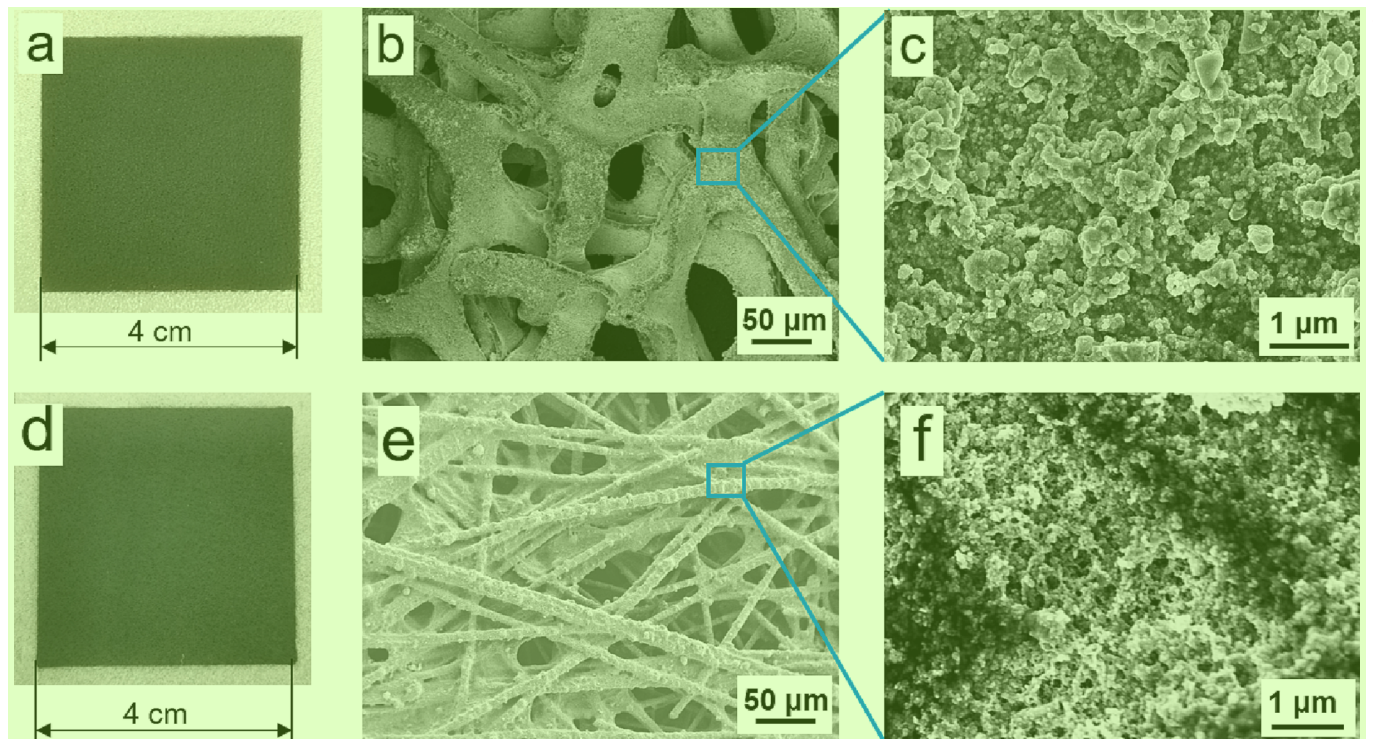


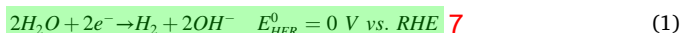
**Fig. 3.** Morphology and microstructure of as-prepared CCS electrodes. a-c) Photo and SEM images of CCS anode with  $1.0 \text{ mg cm}^{-2}$   $\text{IrO}_2$  and 12.5 wt% AEI. d-f) Photo<sup>2</sup> and SEM images of CCS cathode with  $1.0 \text{ mg cm}^{-2}$   $\text{Pt/C}$  and 25 wt% AEI.

<sup>3</sup> °C from the damage of polymer backbone [20]. Moreover, the DMA result indicates that the PBPA AEM has a glass transition temperature ( $T_g$ ) as high as 175 °C. Above all, the as-synthesized PBPA AEM shows high ionic conductivity, low  $\text{H}_2$  permeability and excellent thermal stability, which are favorable for the AEMWE.

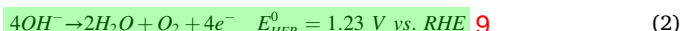
<sup>4</sup> Fig. 3 displays photos and surface SEM images of CCS electrodes with an area of  $4 \times 4 \text{ cm}^2$ . The anode consists of a catalyst layer of  $1.0 \text{ mg cm}^{-2}$   $\text{IrO}_2$  and 12.5 wt% AEI covered on 0.2 mm-thick nickel foam. Similarly, the cathode consists of a catalyst layer of  $1.0 \text{ mg cm}^{-2}$   $\text{Pt/C}$  and 25 wt% AEI covered on hydrophilic carbon paper. Distinctly, both electrodes process uniform catalyst coating (Fig. 3ad) and well dispersed nanoparticles. The anode catalyst layer is relatively compact while the cathode catalyst layer is more porous (Fig. 3bcf). The ECSA of the anode and cathode, measured via the double layer capacitance method (Fig. S4), is 2.7 and  $20.3 \text{ cm}^2$  respectively.

### 3.2. Water electrolysis performance for various electrolyte solution<sup>5</sup>

Generally, when an AEMWE cell is operated, alkaline hydrogen evolution reaction (HER) occurs in the cathode, which produces hydrogen and  $\text{OH}^-$  ions:



The  $\text{H}_2\text{O}$  molecules are provided by the operating solution, while the electrons are generated from the anode reaction and transported via the external circuit. The produced  $\text{OH}^-$  ions migrate through the AEM to the anode. In the anode catalyst layer,  $\text{OH}^-$  ions participate in the oxygen evolution reaction (OER) to produce oxygen, water, and electrons:



It is worth noticing that, due to the irreversible loss of the OER, the onset voltage of the AEMWE cell is about 1.23 V [33,34].

The pH, ionic conductivity and viscosity of the solution strongly depend on the type of electrolyte solution, therefore, changing the type of electrolyte solution could result in dominant influences on the

<sup>3</sup> microscopic physical and chemical processes [18,35–37]. When the AEMWE is operated in pure water, the  $\text{OH}^-$  ions can only transport via the AEI and AEM, and thus the HER and OER reactions occur only at the three-phase boundaries among the catalytic surface, AEI and pure water. When the electrolyte solution is changed to KOH or NaOH solution, the ionic conduction pathway is extended to the liquid solution, and thus the reaction could occur at the liquid/catalyst interface. When saturated  $\text{NaHCO}_3$  solution is used, although it also provides efficient ionic pathway in liquid phase, the membrane resistance, electrode potentials and anode charge transfer resistance will be significantly increased due to: 1) the charge carriers in the AEM are turned to be sluggish  $\text{HCO}_3^-$  and  $\text{CO}_3^{2-}$  ions; 2) since the  $\text{NaHCO}_3$  solution is nearly neutral, both the anode and cathode potentials would be elevated by about 0.41 V as compared to the KOH/NaOH-operated ones; 3) the bicarbonate/carbonate ions can further result in competitive adsorptions at the anode against  $\text{OH}^-$  ions.

<sup>4</sup> Fig. 4a shows the polarization curves of the AEMWE cells operated with saturated  $\text{NaHCO}_3$ , pure water, 1.0 M NaOH and 1.0 M KOH solutions, respectively. At the voltage of 2.0 V, current densities achieved by the cells sequentially were 0.3, 0.6, 2.0, and  $2.8 \text{ A cm}^{-2}$ . Overall, the cell operated with 1.0 M KOH solution exhibited the highest performance, while the two cells that were operated with the saturated  $\text{NaHCO}_3$  solution and pure water exhibited poor performance. In the low current density range (less than  $0.2 \text{ A cm}^{-2}$ ), the cells that were operated with saturated  $\text{NaHCO}_3$  solution and pure water exhibited higher voltages than those operated with alkali solutions, indicating higher activation overpotentials of the electrodes. In the higher current density range ( $>0.2 \text{ A cm}^{-2}$ ), the voltage slopes varied from each other significantly, indicating the considerable difference in the internal resistances.

<sup>5</sup> The Nyquist plots of the EIS data of the cells are shown in Fig. 4b, and the area specific charge transfer resistance (ASCTR) and area specific ohmic resistance (ASOR) of the cells are further identified and shown in Fig. 4c. Both the ASCTR and ASOR of the cell operated with pure water were higher than those of the cells operated with the NaOH and KOH solutions, which can be attributed to the absence of ionic conduction

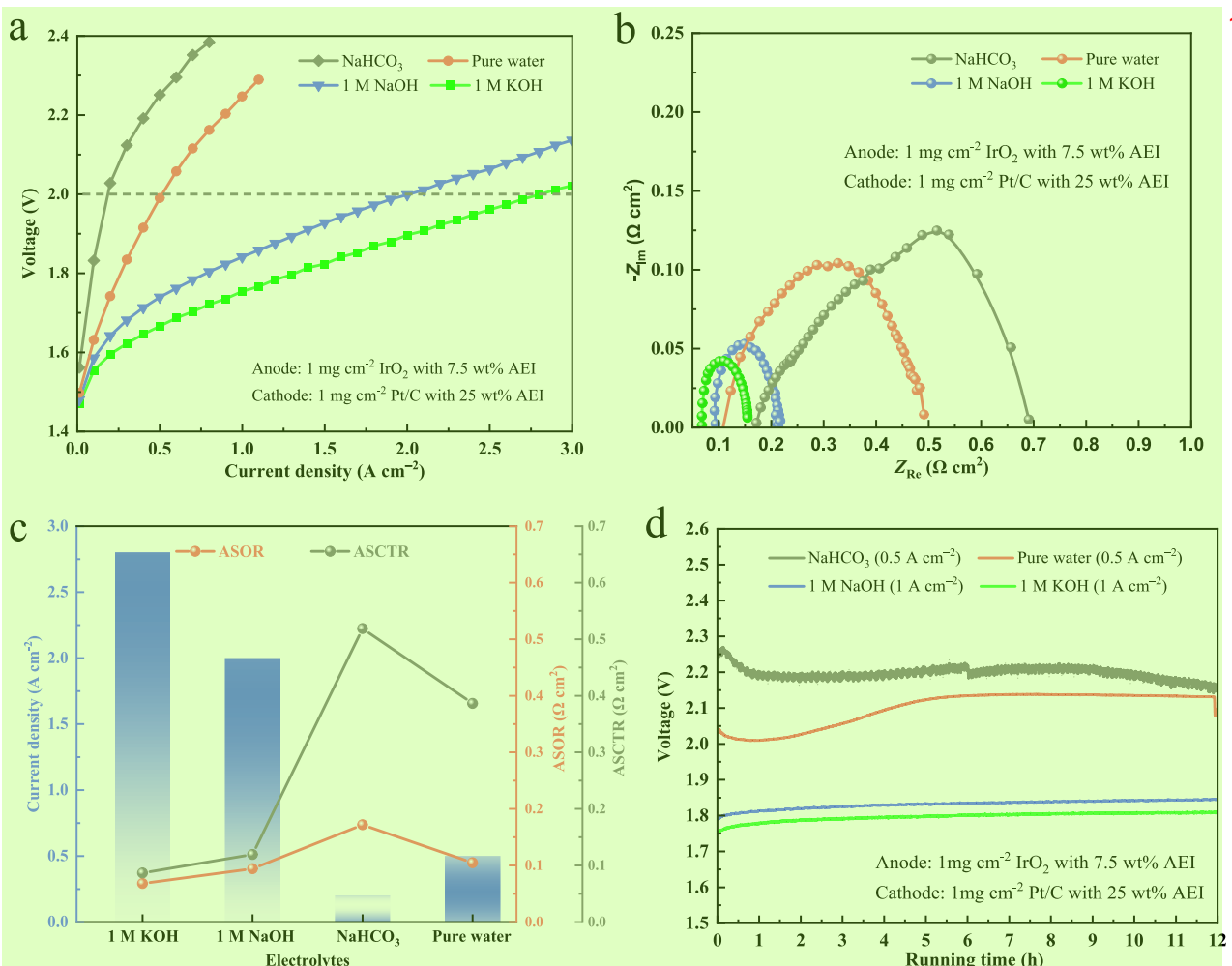


**Fig. 4.** The water electrolysis performance of AEMWE cell for various electrolyte solutions including pure water, saturated  $\text{NaHCO}_3$ , 1.0 M NaOH and 1.0 M KOH solutions. a) Polarization curves. b) Nyquist plots, c) Current density, ASOR, and ASCTR. d) Voltage behavior during the 12-h CCS test. All tests were at 60 °C.

pathway in the pure water and the limited area of effective electrochemical surface. Although the saturated  $\text{NaHCO}_3$  solution provided more efficient ionic pathway than the pure water did, even higher ASCTR and ASOR were observed. Such poor performance can be due to the retarded OER kinetics by the competitive adsorption against  $\text{OH}^-$  ions and the reduction in the membrane conductivity that are induced by the bicarbonate/carbonate poisoning.

Fig. 4d presents the voltage behaviors of the cells during 12-h CCE tests. The current density for the cells operated with pure water and saturated  $\text{NaHCO}_3$  solution was  $0.5 \text{ A cm}^{-2}$ , while the current density for the KOH and NaOH-operated cells was  $1.0 \text{ A cm}^{-2}$ . The voltage of the pure water-operated cell was around 2.05 V at the beginning, which decreased gradually to 2.0 V. This voltage decrement was attributed to an activation of the MEA by the cathode-generated  $\text{OH}^-$  ions. Then, the voltage increased continuously for four hours and reached 2.1 V, which can be mainly attributed to the phenyl oxidation process of the anode AEI [38]. In the last hours, the voltage remained stable at 2.1 V, which indicates that the MEA became stabilized after the anode AEI oxidation. The initial voltage of the cell operated with saturated  $\text{NaHCO}_3$  solution was higher than that of the pure water-operated cell, which was around 2.25 V. The oxidation of the anode AEI was drastic and thus a voltage increment was clearly observed in the first minutes. The voltage decrement induced by the MEA activation process was also observed in the first hour. In the following hours, instead of any increment, a decrement in voltage occurred at the eighth hour. Meanwhile, the cells that were operated with KOH and NaOH exhibited relatively stable

voltage behavior during the short-term operation, which were around 1.79 V and 1.82 V, respectively (Fig. 4d). The much more stabilized cell voltage, as compared to the cells operated with pure water and saturated  $\text{NaHCO}_3$  solution, can be attributed to the fact that, the AEI was more chemically stabilized at the low anode potential.

Above all, the AEMWE cells with the PBPA AEM stably operated with 1.0 M KOH, NaOH solutions and pure water in the 12-h duration of CCE. Using 1.0 M KOH or NaOH solution as the electrolyte can improve the cell performance and durability [18]. In the 12-h CCE test, the KOH-operated cell exhibited the highest performance, which was 1.79 V @  $1.0 \text{ A cm}^{-2}$ .

### 3.3. Effect of AEI contents

In the AEMWE cells, the AEI was employed in the electrodes for two functions: 1) robustly binding the catalyst nanoparticles to form the porous structure, and attaching the catalyst layer to the substrate, and 2) efficiently conducting  $\text{OH}^-$  ions between the catalyst and AEM. Insufficient AEI content results in not only poor mechanical stability of the catalyst layer results from, but also low effective ionic conductivity and thus limited utilization of the catalyst. On the other hand, excessive AEI content will lead to a dense structure that resists the gaseous and liquid flows, and even increase the contact resistance between the catalyst particles. Therefore, appropriate anode and cathode AEI contents in the MEA could be important to improving the cell performance and durability [39–44].

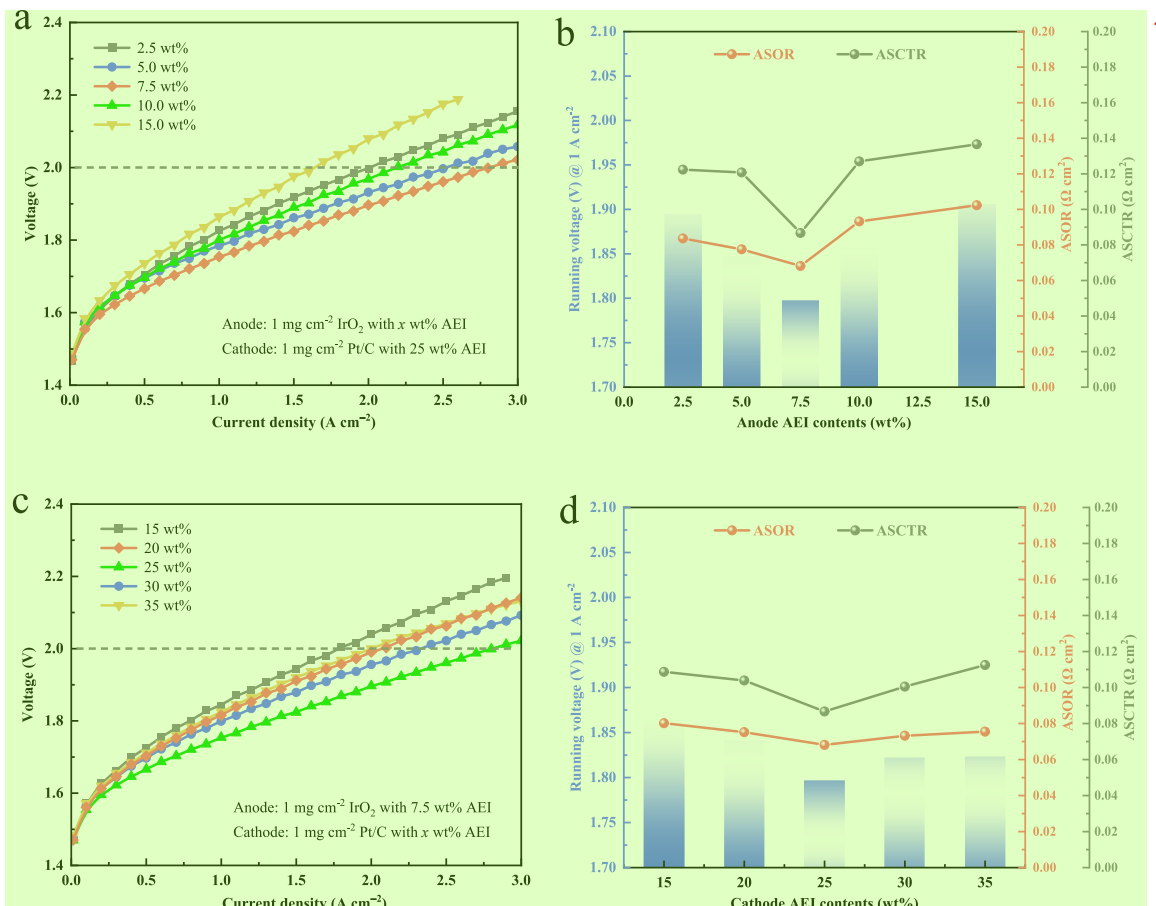


**Fig. 5.** The effect of AEI contents on the water electrolysis performance of AEMWE cells. a) The polarization curves with various anode AEI contents. b) The running voltage, ASOR and ASCTR with various anode AEI contents. c) The polarization curves with various cathode AEI contents. d) The running voltage, ASOR and ASCTR with various cathode AEI contents. All tests were in 1.0 M KOH at 60 °C.

Fig. 5a presents the polarization curves of the AEMWE cells with anode AEI contents of 2.5, 5.0, 7.5, 10.0, and 15.0 wt%, respectively. As the anode AEI content increased from 2.5 to 7.5 wt%, the current density at 2.0 V increased from 2.0 to 2.8  $\text{A cm}^{-2}$ . With further increments in the anode AEI content to 10 and 15 wt%, the current density was reduced to 2.2 and 1.7  $\text{A cm}^{-2}$ , respectively. Such trend of the cell performance changing with the anode AEI content was further confirmed in the CCE test (Fig. S5). The ASOR and ASCTR of the cells are summarized in Fig. 5b, and the EIS curves presented in Fig. S6. Both the ASOR and ASCTR were reduced when the anode AEI content increased, from 0.084 and 0.122 to 0.068 and 0.087  $\Omega \text{ cm}^2$ . With the further increment of the anode AEI content by 2.5 wt%, the ASOR and ASCTR dramatically increased to 0.093 and 0.127  $\Omega \text{ cm}^2$ , which indicates that this anode AEI content might be excessive and thus isolated catalyst nanoparticles were formed.

Fig. 5c presents the polarization curves of the AEMWE cells with various cathode AEI contents, which were 15, 20, 25, 30, and 35 wt%, respectively. Performance of the AEMWE cells was gradually improved as the cathode AEI content increased from 15 to 25 wt%, and was lowered gradually with further increments to 35 wt%. It could be seen from Fig. 5d that the variation of the cathode AEI content more significantly affected the ASCTR (Fig. S7).

In the comparison between the effects of the anode and cathode AEI contents, it can be found that the cell performance was more sensitive to the anode AEI content than the cathode AEI content. A reasonable explanation is that, due to the high density of the anode catalyst, a change in the weight ratio of AEI results in a large change in the volume fraction.

### 3.4. Effect of KOH concentration and temperature

The electrolyte concentration is important, because it also determines the reaction kinetics, internal resistance, and effective electrochemical surface area [16,18,45]. Fig. 6a shows the polarization curves of the AEMWE cells that were operated with various KOH concentrations, i.e., 0.1, 0.5, and 1.0 M. As the KOH concentration increases, the performance was significantly improved. The current densities at 2.0 V are 1.3, 1.8 and 2.8  $\text{A cm}^{-2}$  for 0.1, 0.5, and 1.0 M KOH, respectively. According to the ASCTR and ASOR data shown in Fig. S8 and Fig. S9, both the ionic conduction and the reaction kinetics were accelerated with the increment in the KOH concentration. Fig. 6b shows the voltage behaviors of the AEMWE cells in the CCE test. The cell voltage with 0.1, 0.5 and 1.0 M KOH were around 1.95, 1.86 and 1.79 V, respectively. It is known that the higher KOH concentration increases the ionic conductivity in the liquid electrolyte, and thus reduces the voltage loss consumed by the ionic conduction. Meanwhile, the enhanced ionic pathway can promote the overall utilization of the catalyst and thus reduce the electrode overpotential.

In the practical operation, the single cell voltage ( $U_{\text{cell}}$ ) of AEMWE is determined by not only the theoretical voltage of water electrolysis ( $E_{\text{OER}}^0 - E_{\text{HER}}^0$ ), but also the overpotentials of the anode and cathode ( $\eta_a$  and  $\eta_c$ ), as well as the ohmic loss ( $iR_\Omega$ , where  $R_\Omega$  represents the internal resistance):

$$U_{\text{cell}} = (E_{\text{OER}}^0 - E_{\text{HER}}^0) + \eta_a + \eta_c + iR_\Omega \quad (3)$$

As the temperature increases, the resulting ohmic loss and electrode overpotentials could be reduced, since the ion migration in the

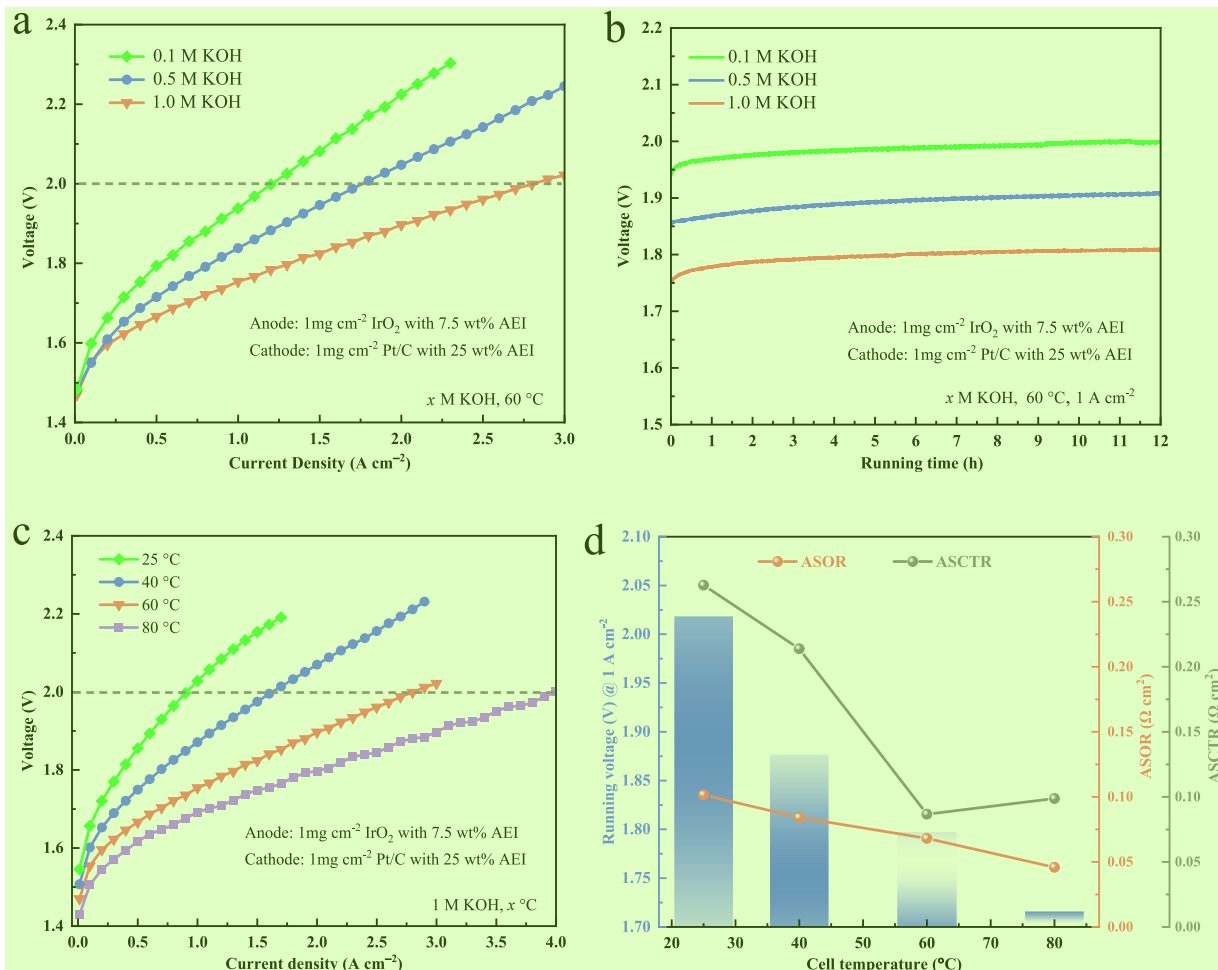


**Fig. 6.** The effect of KOH concentration and operating temperature on the water electrolysis performance of AEMWE cells. a) The polarization curves of the cells operated with 0.1, 0.5 and 1.0 M KOH solutions, b) The voltage behavior of the cells during the 12-h CCS test. c) The polarization curves of the cells operated at the operating temperatures of 25, 40, 60 and 80 °C. d) The running voltage during the CCS test, ASOR and ASCTR under the various temperatures. 1 2

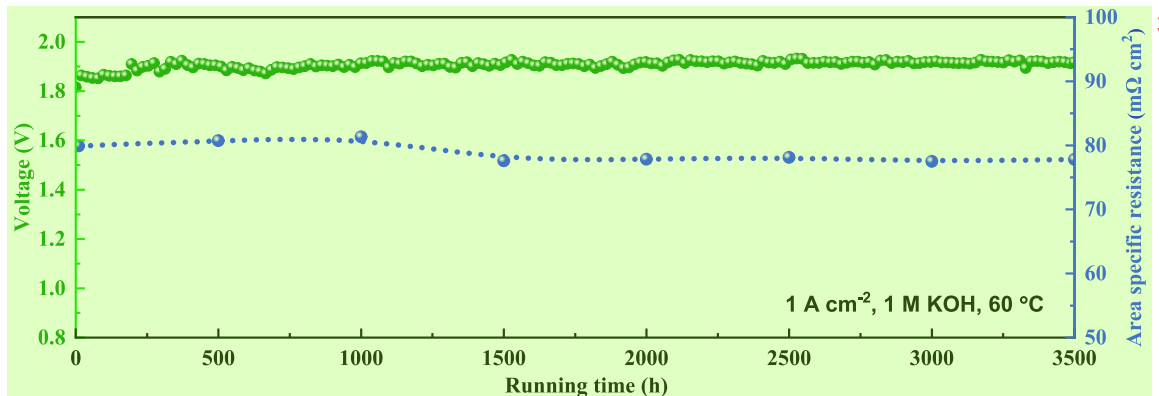


**Fig. 7.** The voltage and internal resistance behavior of PBPA-based AEMWE cell during the 3,500-h CCS test (still running). 4

electrolytes and the electron transfer at the electrochemical surface are accelerated [39]. However, the operating temperature of an AEMWE cell is limited by the thermal stability of the AEM. An extremely high temperature will lead to the decomposition of the functional groups from the AEM and a dramatic drop in the ionic selectivity, which shortens the long-term durability [45–47].

The AEMWE cells with the PBPA AEM were operated at various operating temperatures, i.e., 25, 40, 60, and 80 °C, respectively. As presented in Fig. 6c, the cell performance was clearly elevated with the

increase in the operating temperature. At the voltage of 2 V, the current densities were 0.9, 1.6, 2.8, and 4.0 A cm<sup>-2</sup> at 25, 40, 60, and 80 °C respectively. As shown in Fig. 6d, as the temperature increases from 25 to 60 °C, the ASOR and ASCTR decreased gradually from 101 and 263 mΩ cm<sup>2</sup> to 68 and 87 mΩ cm<sup>2</sup> (Fig. S10). This indicates that the elevated performance benefited from the accelerated ion migration and reaction kinetics. However, as the operating temperature further increases to 80 °C, the ASCTR slightly increased. This might resulted from the enhanced cation crossover at the high temperature, which led to a 5 7

**Table 2**  
Long-term ( $\geq 500$  h) performance of state-of-the-art AEMWE cells.

AEMs	catalyst loading ( $\text{mg cm}^{-2}$ )		MEA type	electrolyte	T ( $^{\circ}\text{C}$ )	$J (\text{A cm}^{-2})$	$E_{\text{cell}}$ (V)	Time (h)	Deg. rate ( $\mu\text{V h}^{-1}$ )	Ref.
	Anode	Cathode								
ATM-PP	$\text{IrO}_2$ , 3.0	Pt black, 1.0	CCM	$\text{H}_2\text{O}$	50	0.2	2.2–2.5	2100	143	[27]
HTMA-DAPP	$\text{Co}_3\text{O}_4$ , 3.0	Pt/C, 3.0	CCM	1 wt% $\text{K}_2\text{CO}_3$	50	0.5	1.9–2.1	750	130	[18]
A-201 Tokuyama	$\text{IrO}_2$ , 2.6	Pt black, 2.4	CCS	$\text{H}_2\text{O}$	50	0.2	2.0–2.25	535	467	[50]
PFTP-13	$\text{IrO}_2$ , 2.0	Pt/C, 0.5	CCM	1 M KOH	80	0.5	2.1	1100	200	[48]
Sustainion X37-50	$\text{NiFe}_2\text{O}_4$ , 1.8	Raney nickel, 2.7	CCS	1 M KOH	60	1.0	1.85–1.90	10,100	1	[49]
Sustainion Grade-T	$\text{NiFe}_2\text{O}_4$ , 1.8	Raney nickel, 14.5	CCS	1 M KOH	60	1.0	1.80–1.86	12,180	1	[49]
PBPA	$\text{IrO}_2$ , 1.0	Pt/C, 1.0	CCS	1 M KOH	60	1.0	1.88–1.92	3,500	6.5	This work
PBPA	$\text{NiFe}_2\text{O}_4$ , 1.5	Pt/C, 1.0	CCS	1 M KOH	60	1.0	1.70–1.9	1,500	32.4	This work

reduction of  $\text{OH}^-$  concentration in the anode. In the CCE test, the voltage of the AEMWE cell could be maintained at 1.7 V at 80 °C, as shown in Fig. S11.

### 3.5. Long-term durability of PBPA-based AEMWE

To further evaluate the performance and durability of this AEMWE cell, the CCE test was performed at  $1.0 \text{ A cm}^{-2}$  for more than 3500 h. Fig. 7 shows the behaviors of the voltage and internal resistance of this cell. In the first 200 h, a gradual increment in the cell voltage occurred till reaching 1.9 V, which indicates the phenyl oxidation in the anode still happened with the optimized parameters [38]. After this stage, the voltage was maintained in the range between 1.88 and 1.92 V, corresponding to the voltage efficiency ranging between 65.4 and 64.1%. Despite the first 200 h, the voltage was almost steady around 1.9 V. The performance degradation rate was calculated to be less than  $6.5 \mu\text{V h}^{-1}$ , as given in Fig. S12. The internal resistance almost remained around  $79 \text{ m}\Omega \text{ cm}^2$  stably during the whole duration, which basically shall be attributed to the high ionic conductivity and chemical stability of the PBPA AEM.

Table 2 summarized the long-term performance of state-of-the-art AEMWE cells reported recently, which were operated over 500 h. It is found that most of the cells exhibited a high voltage of over 1.9 V, even under relatively low current densities. To the best of our knowledge, the present AEMWE cell with the PBPA AEM is among the only three cells that can stably work at  $1.0 \text{ A cm}^{-2}$  for thousands of hours [27,48,49], and the voltage can maintain around 1.9 V with a low voltage rising rate of  $6.5 \mu\text{V h}^{-1}$ . The PBPA cell equipped with the nonprecious anode was also tested. As shown in Fig. S13a, at each current density, voltage of this nonprecious cell was slightly lower than the precious one, which indicates that performance of the nonprecious anode is comparable to the  $\text{IrO}_2$  one towards alkaline OER. In the 1,500-h CCE test, the cell voltage steadily maintained between 1.7 ~ 1.9 V (Fig. S13b). As the cell performance depends on not only the AEM properties, but also the MEA fabrication technique and other key materials (catalysts, ionomer, and substrates), the performance of the PBPA-based cell is expected be improved by the development of high-performance electrodes in the future. From these, the PBPA AEM and its MEA, which show excellent stability in the long-term CCS AEMWE test, should have great potential for industrial AEMWE systems.

## 4. Conclusions

In summary, this study demonstrated the application of PBPA in the water electrolysis for durable and highly-efficient hydrogen production. The PBPA was synthesized for both AEM and AEI. The AEI contents have great effects on the internal resistance of AEMWE cell, which initially decreases and then increases with the increment of the AEI contents. The cell with the optimal AEI contents of 7.5 wt% (anode) and 25 wt% (cathode) achieves high current densities of 2.8 A and  $4.0 \text{ A cm}^{-2}$  under 2.0 V in 1 M KOH solution at 60 and 80 °C, respectively. Meanwhile, the PBPA-based MEA has good water electrolysis performance in pure water and  $\text{NaHCO}_3$  solution. Moreover, the water electrolysis performance

strongly depends on the KOH concentration and temperature. The PBPA-based AEMWE cell show excellent durable water electrolysis performance in 1 KOH solution at  $1.0 \text{ A cm}^{-2}$  and 60 °C. The cell voltage maintains around 1.9 V for over 3500 h CCE test, with a rising rate of less than  $6.5 \mu\text{V h}^{-1}$ . Therefore, the PBPA-based AEM and MEA show outstanding durability and efficiency in the AEMWE, and have a great potential for industrial hydrogen production via the AEMWE.

## Declaration of Competing Interest

The authors declare that they have no known competing financial interests or personal relationships that could have appeared to influence the work reported in this paper.

## Data availability

Data will be made available on request.

## Acknowledgments

This work is supported by the National Nature Science Foundation of China (No. 22178292), Science and Technology Planning Project of Fujian Province of China (No. 2020H0003), and Science and Technology Planning Project of Xiamen City of China (No. 3502Z20206050).

## Appendix A. Supplementary data

Supplementary data to this article can be found online at <https://doi.org/10.1016/j.cej.2023.143442>.

## References

- [1] S. Chu, Y. Cui, N. Liu, The path towards sustainable energy, *Nat. Mater.* 16 (1) (2016) 16–22.
- [2] A.G. Olabi, M.A. Abdelkareem, Renewable energy and climate change, *Renew. Sust. Energ. Rev.* 158 (2022) 112111.
- [3] M.F. Lagadec, A. Grimaud, Water electrolyzers with closed and open electrochemical systems, *Nat. Mater.* 19 (11) (2020) 1140–1150.
- [4] M. Chatenet, B.G. Pollet, D.R. Dekel, et al., Water electrolysis: from textbook knowledge to the latest scientific strategies and industrial developments, *Chem. Soc. Rev.* 51 (11) (2022) 4583–4762.
- [5] A. Buttler, H. Spleithoff, Current status of water electrolysis for energy storage, grid balancing and sector coupling via power-to-gas and power-to-liquids: a review, *Renew. Sust. Energ. Rev.* 82 (2018) 2440–2454.
- [6] Z.-Y. Yu, Y.u. Duan, X.-Y. Feng, X. Yu, M.-R. Gao, S.-H. Yu, Clean and affordable hydrogen fuel from alkaline water splitting: past, recent progress, and future prospects, *Adv. Mater.* 33 (31) (2021) e2007100.
- [7] S. Shiva Kumar, H. Lim, An overview of water electrolysis technologies for green hydrogen production, *EnergyChem* 8 (2022) 13793–13813.
- [8] S.M. Xie WF, Alkaline water electrolysis for efficient hydrogen production, *J. Electrochem.* 28(10) (2022) 22014008.
- [9] N. Du, C. Roy, R. Peach, M. Turnbull, S. Thiele, C. Bock, Anion-exchange membrane water electrolyzers, *Chem. Rev.* 122 (13) (2022) 11830–11895.
- [10] Q. Xu, L. Zhang, J. Zhang, et al., Anion exchange membrane water electrolyzer: electrode design, lab-scaled testing system and performance evaluation, *EnergyChem* 4 (5) (2022), 100087.
- [11] C. Li, J.-B. Baek, The promise of hydrogen production from alkaline anion exchange membrane electrolyzers, *Nano Energy* 87 (2021), 106162.

- [12] C. Santoro, A. Lavacchi, P. Mustarelli, V. Di Noto, L. Elbaz, D.R. Dekel, F. Jaouen, What is next in anion-exchange membrane water electrolyzers? Bottlenecks, benefits, and future, *ChemSusChem* 15 (8) (2022) e202200027.
- [13] M.S. Cha, J.E. Park, S. Kim, S.-H. Han, S.-H. Shin, S.H. Yang, T.-H. Kim, D.M. Yu, S. So, Y.T. Hong, S.J. Yoon, S.-G. Oh, S.Y. Kang, O.-H. Kim, H.S. Park, B. Bae, Y.-E. Sung, Y.-H. Cho, J.Y. Lee, Poly(carbazole)-based anion-conducting materials with high performance and durability for energy conversion devices, *Energy Environ. Sci.* 13 (10) (2020) 3633–3645.
- [14] P. Fortin, T. Khoza, X. Cao, et al., High-performance alkaline water electrolysis using Aemion™ anion exchange membranes, *J. Power Sources* 451 (2020), 227814.
- [15] A. Khataee, A. Shirole, P. Jannasch, A. Krüger, A. Cornell, Anion exchange membrane water electrolysis using Aemion™ membranes and nickel electrodes, *J. Mater. Chem. A* 10 (30) (2022) 16061–16070.
- [16] D. Li, E.J. Park, W. Zhu, Q. Shi, Y. Zhou, H. Tian, Y. Lin, A. Serov, B. Zulevi, E. D. Baca, C.y. Fujimoto, H.T. Chung, Y.S. Kim, Highly quaternary polystyrene ionomers for high performance anion exchange membrane water electrolyzers, *Nat. Energy* 5 (5) (2020) 378–385.
- [17] D. Henkensmeier, M. Najibah, C. Harms, et al., Overview: State-of-the art commercial membranes for anion exchange membrane water electrolysis, *J. Electrochem. Energy* 18 (2) (2021), 024001.
- [18] D. Li, A.R. Motz, C. Bae, C.y. Fujimoto, G. Yang, F.-Y. Zhang, K.E. Ayers, Y.S. Kim, Durability of anion exchange membrane water electrolyzers, *Energy Environ. Sci.* 14 (6) (2021) 3393–3419.
- [19] A.R. Cruz, M.C.G. Hernandez, M.T. Guzmán-Gutiérrez, M.G. Zolotukhin, S. Fomine, S.L. Morales, H. Kricheldorf, E.S. Wilks, J. Cárdenas, M. Salmón, Precision synthesis of narrow polydispersity, ultrahigh molecular weight linear aromatic polymers by A2 + B2 nonstoichiometric step-selective polymerization, *Macromolecules* 45 (17) (2012) 6774–6780.
- [20] W.H. Lee, Y.S. Kim, C. Bae, Robust hydroxide ion conducting poly(biphenyl alkylene)s for alkaline fuel cell membranes, *ACS Macro Lett.* 4 (8) (2015) 814–818.
- [21] W.H. Lee, E.J. Park, J. Han, et al., Poly(terphenylene) anion exchange membranes: the effect of backbone structure on morphology and membrane property, *ACS Macro Lett.* 6 (5) (2017) 566–570.
- [22] C. Hu, Q. Zhang, C. Lin, Z. Lin, L. Li, F. Soyekwo, A. Zhu, Q. Liu, Multi-cation crosslinked anion exchange membranes from microporous Tröger's base copolymers, *J. Mater. Chem. A* 6 (27) (2018) 13302–13311.
- [23] E.J. Park, C.B. Capuano, K.E. Ayers, C. Bae, Chemically durable polymer electrolytes for solid-state alkaline water electrolysis, *J. Power Sources* 375 (2018) 367–372.
- [24] S.Y. Kang, J.E. Park, G.Y. Jang, O.-H. Kim, O.J. Kwon, Y.-H. Cho, Y.-E. Sung, High-performance and durable water electrolysis using a highly conductive and stable anion-exchange membrane, *Int. J. Hydrogen Energy* 47 (15) (2022) 9115–9126.
- [25] A.D. Mohanty, S.E. Tignor, J.A. Krause, Y.-K. Choe, C. Bae, Systematic alkaline stability study of polymer backbones for anion exchange membrane applications, *Macromolecules* 49 (9) (2016) 3361–3372.
- [26] M.R. Hibbs, Alkaline stability of poly(phenylene)-based anion exchange membranes with various cations, *J. Polym. Sci. Pol. Phys.* 51 (24) (2013) 1736–1742.
- [27] Y.K. Choe, C. Fujimoto, K.-S. Lee, et al., Alkaline stability of benzyl trimethyl ammonium functionalized polyaromatics: a computational and experimental study, *Chem. Mater.* 26 (19) (2014) 5675–5682.
- [28] M.G. Marino, K.D. Kreuer, Alkaline stability of quaternary ammonium cations for alkaline fuel cell membranes and ionic liquids, *ChemSusChem* 8 (3) (2015) 513–523.
- [29] E.J. Park, S. Komini Babu, Y.S. Kim, Gas permeability test protocol for ion-exchange membranes, *Front. Energy Res.* 10 (2022), 945654.
- [30] C. Wei, R.R. Rao, J. Peng, B. Huang, I.E.L. Stephens, M. Risch, Z.J. Xu, Y. Shao-Horn, Recommended practices and benchmark activity for hydrogen and oxygen electrocatalysis in water splitting and fuel cells, *Adv. Mater.* 31 (31) (2019) e1806296.
- [31] C. Wei, S. Sun, D. Mandler, X. Wang, S.Z. Qiao, Z.J. Xu, Approaches for measuring the surface areas of metal oxide electrocatalysts for determining their intrinsic electrocatalytic activity, *Chem. Soc. Rev.* 48 (9) (2019) 2518–2534.
- [32] C. Huang, P.K. Chu, Recommended practices and benchmarking of foam electrodes in water splitting, *Trends Chem.* 4 (12) (2022) 1065–1077.
- [33] S. Siracusano, V. Baglio, N. Briguglio, G. Brunaccini, A. Di Blasi, A. Stassi, R. Ornelas, E. Trifoni, V. Antonucci, A.S. Aricò, An electrochemical study of a PEM stack for water electrolysis, *Int. J. Hydrogen Energy* 37 (2) (2012) 1939–1946.
- [34] C. Lamy, P. Millet, A critical review on the definitions used to calculate the energy efficiency coefficients of water electrolysis cells working under near ambient temperature conditions, *J. Power Sources* 447 (2020), 227350.
- [35] A. Kiessling, J.C. Fornaciari, G. Anderson, X. Peng, A. Gerstmayer, M.R. Gerhardt, S. McKinney, A. Serov, Y.S. Kim, B. Zulevi, A.Z. Weber, N. Danilovic, Influence of supporting electrolyte on hydroxide exchange membrane water electrolysis performance: analyte, *J. Electrochem. Soc.* 168 (8) (2021) 084512.
- [36] A.K. Niaz, J.-Y. Park, H.-T. Lim, Operational parameters correlated with the long-term stability of anion exchange membrane water electrolyzers, *Int. J. Hydrogen Energy* 46 (62) (2021) 31550–31562.
- [37] A. Kiessling, J.C. Fornaciari, G. Anderson, X. Peng, A. Gerstmayer, M. Gerhardt, S. McKinney, A. Serov, A.Z. Weber, Y.S. Kim, B. Zulevi, N. Danilovic, Influence of supporting electrolyte on hydroxide exchange membrane water electrolysis performance: catholyte, *J. Electrochem. Soc.* 169 (2) (2022) 024510.
- [38] D. Li, I. Matanovic, A.S. Lee, E.J. Park, C.y. Fujimoto, H.T. Chung, Y.S. Kim, Phenyl oxidation impacts the durability of alkaline membrane water electrolyzer, *ACS Appl. Mater. Interfaces* 11 (10) (2019) 9696–9701.
- [39] A. Lim, H.-J. Kim, D. Henkensmeier, S. Jong Yoo, J. Young Kim, S.O. Young Lee, Y.-E. Sung, J.H. Jang, H.S. Park, A study on electrode fabrication and operation variables affecting the performance of anion exchange membrane water electrolysis, *J. Ind. Eng. Chem.* 76 (2019) 410–418.
- [40] N. Chen, Y.M. Lee, Anion exchange polyelectrolytes for membranes and ionomers, *Prog. Polym. Sci.* 113 (2021), 101345.
- [41] S. Koch, P.A. Heizmann, S.K. Kilian, B. Britton, S. Holdcroft, M. Breitwieser, S. Vierrath, The effect of ionomer content in catalyst layers in anion-exchange membrane water electrolyzers prepared with reinforced membranes (Aemion+™), *J. Mater. Chem. A* 9 (28) (2021) 15744–15754.
- [42] E. Cossar, F. Murphy, J. Walia, et al., Role of ionomers in anion exchange membrane water electrolysis: is aemion the answer for nickel-based anodes? *ACS Appl. Energy Mater.* 5 (8) (2022) 9938–9951.
- [43] M. Plevová, J. Hnát, J. Žitka, et al., Optimization of the membrane electrode assembly for an alkaline water electrolyser based on the catalyst-coated membrane, *J. Power Sources* 539 (2022), 231476.
- [44] K. Yassin, I.G. Rasin, S. Brandon, et al., Elucidating the role of anion-exchange ionomer conductivity within the cathode catalytic layer of anion-exchange membrane fuel cells, *J. Power Sources* 524 (2022), 231083.
- [45] I.V. Pushkareva, A.S. Pushkarev, S.A. Grigoriev, P. Modisha, D.G. Bessarabov, Comparative study of anion exchange membranes for low-cost water electrolysis, *Int. J. Hydrogen Energy* 45 (49) (2020) 26070–26079.
- [46] N. Chen, Y.M. Lee, Anion-conducting polyelectrolytes for energy devices, *Trends Chem.* 4 (3) (2022) 236–249.
- [47] H. Khalid, M. Najibah, H.S. Park, C. Bae, D. Henkensmeier, Properties of anion exchange membranes with a focus on water electrolysis, *Membranes* 12 (10) (2022) 989.
- [48] N. Chen, S.Y. Paek, J.Y. Lee, J.H. Park, S.Y. Lee, Y.M. Lee, High-performance anion exchange membrane water electrolyzers with a current density of 7.68 A cm<sup>-2</sup> and a durability of 1000 hours, *Energy Environ. Sci.* 14 (12) (2021) 6338–6348.
- [49] B. Motealleh, Z. Liu, R.I. Masel, J.P. Sculley, Z. Richard Ni, L. Meroueh, Next-generation anion exchange membrane water electrolyzers operating for commercially relevant lifetimes, *Int. J. Hydrogen Energy* 46 (5) (2021) 3379–3386.
- [50] Y. Leng, G. Chen, A.J. Mendoza, T.B. Tighe, M.A. Hickner, C.-Y. Wang, Solid-state water electrolysis with an alkaline membrane, *J. Am. Chem. Soc.* 134 (22) (2012) 9054–9057.